Materials Horizons

Embedded 3D Printing of UV-curable Thermosetting Composites with Continuous Fiber

Journal:	*Materials Horizons*
Manuscript ID	MH-COM-06-2024-000705
Article Type:	Communication
Date Submitted by the Author:	04-Jun-2024
Complete List of Authors:	Ding, Yuchen; University of Colorado Denver, Mechanical Engineering Alston, Xavier Gracego; University of Colorado Denver Wang, Yuanrui; University of Colorado Denver Dong, Guoying; University of Colorado Denver Dunn, Martin; University of Colorado Denver, Engineering and Applied Science Yu, Kai; University of Colorado at Denver - Anschutz Medical Campus, Mechanical Engineering

This paper demonstrates the new concept of embedded 3D printing of UV-curable composites with continuous fiber. This approach differentiates from existing studies that rely on extrusion-based printing methods with in-nozzle impregnation mechanisms, which often result in noticeable void density and weak inter-filament bonding strength. In addition, they cannot dynamically control fiber volume fractions and matrix materials during printing, which are significant manufacturing constraints. The newly developed printing method deposits continuous fibers below the resin surface. A laser beam is directed onto the resin surface to simultaneously cure the resin around the fiber and create composites. It produces composite samples with perfectly aligned fibers, minimal void density, and outstanding mechanical properties. It also allows for the adjustment of fiber volume fractions and matrix resin during printing. Moreover, the printing process balances gravitational forces with the buoyancy of filaments in the resin, allowing for the fabrication of hollow structures without support materials. The new printing method is compatible with various commercial resins and continuous fibers. It is anticipated to significantly enhance design freedom, manufacturing capability, and application scopes of 3D printed composites. It can also be extended to other multifunctional composites printed with various active resins and functional fibers.

Embedded 3D Printing of UV-Curable Thermosetting Composites with Continuous Fiber

*Yuchen Ding [1], Alston X. Gracego [1], Yuanrui Wang [1], Guoying Dong [1], Martin L. Dunn [1,] *, Kai Yu [1,] **

[1] Department of Mechanical Engineering, University of Colorado Denver, Denver, CO 80217, USA.

* Email: martin.dunn@ucdenver.edu, kai.2.yu@ucdenver.edu

Abstract: Extrusion-based 3D printing methods with in-nozzle impregnation mechanisms have been extensively employed in the fabrication of continuous fiber composites. This study presents an innovative embedded 3D printing technique that addresses significant challenges associated with existing methods. The technique utilizes a deposition nozzle to precisely write continuous fibers below the resin. A laser beam is directed onto the resin surface, which simultaneously cures the resin around the fiber bundle. The printing method demonstrates its advantages in producing high-quality composite samples with well-aligned fibers, minimized void density, and outstanding mechanical properties. More importantly, it introduces several capabilities that are highly desirable in the fabrication of contemporary composites, but unattainable with existing methods, including the dynamic control of fiber volume fractions and the ability to change matrix materials during printing. Furthermore, it enables the printing of filaments along curved pathways and printing of overhanging filaments for hollow features without support materials. The developed printing method exhibits versatility in working with different commercially available feedstock resins and reinforcement fibers. It is anticipated to be an impactful approach for the future development of thermosetting composites with diverse structural or multifunctional applications.

Keywords: Continuous fiber, UV-curable composites, varying fiber volume fractions; embedded 3D printing, robotic arm 3D printing.

1. Introduction

3D printing, also known as additive manufacturing, offers significant advantages for composite manufacturing. It provides exceptional design flexibility while eliminating the need for a mold to shape the resin and fiber. Consequently, manufacturing costs remain low even for small-quantity production, which makes it particularly suited for rapid prototyping and product development [1, 2].

Current studies on 3D printing of continuous fiber-reinforced polymer (CFRP) composites have primarily focused on extrusion-based methods, such as fused deposition modeling (FDM) and direct ink writing (DIW). In FDM, the continuous fiber bundle (or pre-impregnated fibers) is fed into the printer head along with a thermoplastic filament [3-10]. After in-nozzle impregnation and filament extrusion, the thermoplastic matrix quickly solidifies and adheres to the previous layer.

The development of 3D printing for thermosetting CFRPs is still in its early stages. There have been recent demonstrations of 3D printing epoxy composites using continuous carbon fiber [11-14]. Due to the high molecular weight, the selected epoxy resin maintains a nearly solid state at room temperature. When heated within a deposition nozzle, the resin can be melted with dramatically decreased viscosities and thus can be printed using a process similar to FDM. After printing, the composites are subjected to a post-heating process to fully polymerize the matrix materials. In our recent study [15], an alternative DIW printing method has been developed, where the viscous flow of the resin applies shear stress on the continuous fiber to drive filament extrusion. This printing method is applicable to a broader range of thermally curable resins and continuous fibers.

UV-curable resins offer significant advantages in CFRP 3D printing, including rapid manufacturing with a high fiber volume fraction, reduced energy consumption, precise control over the curing process, and elimination of post-processing steps [15-22]. Continuous Composite Inc. patented the first design of a DIW printer head [23]. Following filament extrusion, the matrix resin is rapidly cured with UV light, which holds the filaments in place as the printer nozzle moves forward. Other studies in the field employ a similar DIW printing method that involves in-nozzle impregnation of continuous fiber [19, 24]. More recently, 3D printing of UV-curable composites has been integrated with a robotic arm to dramatically enhance freedom of motion control and printing capabilities [19, 25, 26].

Despite exciting developments in the field, extrusion-based printing methods for UV-curable CFRPs face several inherent manufacturing constraints that cannot be resolved simply by optimizing printing conditions. Firstly, after filament deposition, the matrix resin spreads, and the embedded fiber bundle tends to loosen or misalign; the composite filaments in the transverse direction are primarily bonded through weak van der Waals interactions; due to their cylindrical geometry, significant voids may form between filaments and adjacent printing layers. These issues substantially compromise the mechanical performance of printed composites.

Secondly, all current printing processes for UV-curable composites share a similar nozzle impregnation mechanism, which does not allow for adjustments in fiber volume fraction or changes in matrix materials during printing, unless cutting the fiber and switching to a different nozzle with a varied inner diameter or containing a different ink. Thirdly, 3D printing of intricate composite structures with larger-scale hollow or overhanging features is challenging. Gravitational forces continuously deform the deposited filaments in the absence of supporting materials. Consequently, the unique design and manufacturing capabilities of 3D printing are not fully utilized for fabricating contemporary composites with highly optimized topology and distributions of continuous fibers and matrix materials.

The combination of continuous fiber placement and vat photopolymerization offers significant potential to tackle persistent challenges in the field. For example, Lu et al. [27] recently demonstrated its ability to print high-quality composite samples. In their approach, the base matrix is printed first with a groove on the surface. After pausing the printing process, a straight fiber bundle is placed into the groove. Finally, the printing of matrix resin is resumed to seal the fiber bundle inside the composite. This hybrid manufacturing process allows for creating composites with minimal void density and robust interlayer bonding.

In this study, we introduce a novel embedded 3D printing method for UV-curable composites with continuous fibers (**Figure 1a**), which enables the automatic fiber placement and simultaneous resin curing during printing with manual intervention. This method utilizes a six-axis robotic arm to guide the motion of the printer head as it precisely deposits continuous fibers within a liquid resin along both straight and curved pathways. A laser beam is directed onto the resin surface, which cures the resin around the fiber bundle to create composite filaments. These filaments can be printed in two different ways: either onto a substrate within the resin tank or without a substrate (**Figure 1b**). In the latter scenario, the printed filaments float within the resin, which effectively

counterbalances gravitational forces and enables the creation of composite structures with hollow features or suspended filaments.

The developed printing method demonstrates its versatility in producing high-quality composite samples with various types of matrix resin and reinforcement fiber. The printed composite lamina exhibits outstanding mechanical performances in both longitudinal and transverse directions. Notably, the printing method allows for dynamic control of the fiber volume fraction during printing by tuning the size of the laser beam, thereby controlling the amount of resin cured around the fiber bundle. It also enables the change of the matrix resin during printing, which dramatically enhances manufacturing flexibility and offers opportunities for fabricating multimaterial functional composites. The developed printing technology is cost-effective and straightforward to set up, making it accessible for other researchers to replicate when designing diverse applications with composites using various matrix resins and continuous fibers.

2. Results and Discussion

2.1 Embedded Printing of Composite Filaments

In this study, we utilize a series of commercially available UV-curable resins (Siraya Tech Inc., San Gabriel, CA) that are commonly used in digital light processing (DLP) printers. All these resins are compatible with the embedded composite printing, despite their various viscosities with distinct cross-linker contents and different incorporated dyes. Two types of continuous fibers are employed, namely a 1k carbon fiber bundle and a polyester-based fiber thread. According to the supplier, their elastic moduli are 174 GPa and 3.5 GPa, respectively. All these feedstock materials are used in their as-received conditions without any chemical treatments.

Our development of the embedded printing method was initially inspired by the stereolithography technique for UV-curable resins. As shown in **Supplementary Video 1**, by scanning a laser beam (5mV, 405 nm) across the resin surface at a speed of 5mm/s, a solid filament is formed immediately with a perfectly straight boundary profile. The width of the filaments (2 mm) is approximately the same as the spot size of the applied laser beam (**Figure 1c**). When printing without a substrate, the filament thickness is measured to be approximately 1 mm. Dynamic mechanical analysis (DMA) measurements reveal that the fully cured matrix material in **Figure 1c** exhibits a glass transition temperature of 56°C and a room temperature modulus of 1.2 GPa.

Subsequently, continuous carbon fiber is introduced into the printer setup for the printing of individual composite filaments (**Supplementary Video 2**). To ensure that the continuous fiber is completely enveloped by the matrix material, it is essential for the depth of the needle tip to be within the curing depth of the resin, which is typically around 1mm. In this study, without investigating its potential influences on the quality of printed composites, we consistently maintain the straight needle tip (15-gauge with a 1.37mm inner diameter) at a depth of 0.3mm below the resin surface throughout all printing processes. This is achieved by calculating the depth of the resin within the tank based on volume and then precisely controlling the shifting distance of the needle from the substrate. It is important to note that the deposition syringe contains no resin; the needle only functions as a feeding tube to guide the transportation of the fiber bundle. To minimize internal reflections of UV light, all components and fixtures of the printer head are coated with black matte paint. Additionally, a small torsion spring is installed on the fiber roller, which applies a tiny tension force to the fiber to prevent significant spreading before the resin is fully cured.

As shown in **Figure 1d**, the printed composite filament exhibits a clearly defined boundary without notable shape distortion. The embedded carbon fiber is well-aligned in the printing direction. The developed printing method provides the capability to adjust the fiber volume fractions by simply regulating the spot size of the applied laser beam. Using a smaller beam size reduces the amount of resin cured around the fiber, which results in a higher fiber volume fraction within the composite filament. The magnitudes of the fiber volume fractions were tested by measuring the density of printed filaments (see the **Experimental Section** for details). Our characterizations suggest that reducing the beam size from 2 mm to 1 mm increases the fiber volume fraction from 3.6% to 9.6%.

When printing composite filaments without a substrate using carbon fiber and a transparent UV-curable resin ("*Clear V2*"), it is observed that the resin below the fiber remains uncured due to the blocking of light transmission by the fiber (see the filament cross-sectional view in **Figure 1d**). This issue persists even at a lower printing speed of 5mm/s. To address it, the use of colored resins ("*Easy Grey*") proves effective because the inclusion of specific dyes promotes light scattering below the fiber. An alternative approach is to introduce short fibers into the resin. For instance, 10 wt.% milled glass fiber (1/32 inch) is added to the transparent resin (**Figure 1e**). The fiber additives are essentially white powders and do not affect the deposition of continuous fiber. They serve to scatter and disperse UV light more effectively, which leads to the successful curing

of the resin below the fiber, as revealed in the filament cross-sectional view.

Another advantage of incorporating milled glass fiber is to enhance the mechanical performance of printed filaments, as illustrated in **Figure S1** (**Supplementary Materials**). Without the addition of milled glass fiber, the composite filament exhibits an initial compliant stress response with a stiffness of only 1.32 GPa before reaching 0.5% engineering strain, which is much lower than the later stage with a stiffness of 4.16 GPa. This is because the resin cures at a relatively slow pace in the absence of glass fiber, which allows the fiber bundle to relax, spread, and develop a slight curvature at the microscale before resin solidification. Consequently, the embedded fiber within the composite filament cannot bear external loads until it is fully extended. By introducing milled glass fiber into the resin, light transmission is enhanced, and the matrix resin cures more rapidly. This, in turn, prevents the undesired curvature of the embedded fiber. As a result, the stress increases monotonically with a near-constant stiffness of 4.01 GPa. It is worth noting that the mechanical strength of the filaments is not observed to increase significantly compared to those without glass fiber because it is dominated by the content of continuous carbon fiber.

Moreover, the printing method is versatile and can be applied to different types of continuous fiber. As shown in **Figure 1f**, a composite filament is printed with a polyester fiber thread with a 2.1% fiber volume fraction. Due to the small diameter of the fiber thread (0.3mm), its blocking effect on light transmission is negligible, so the resin can be fully cured without the need for adding milled glass fiber.

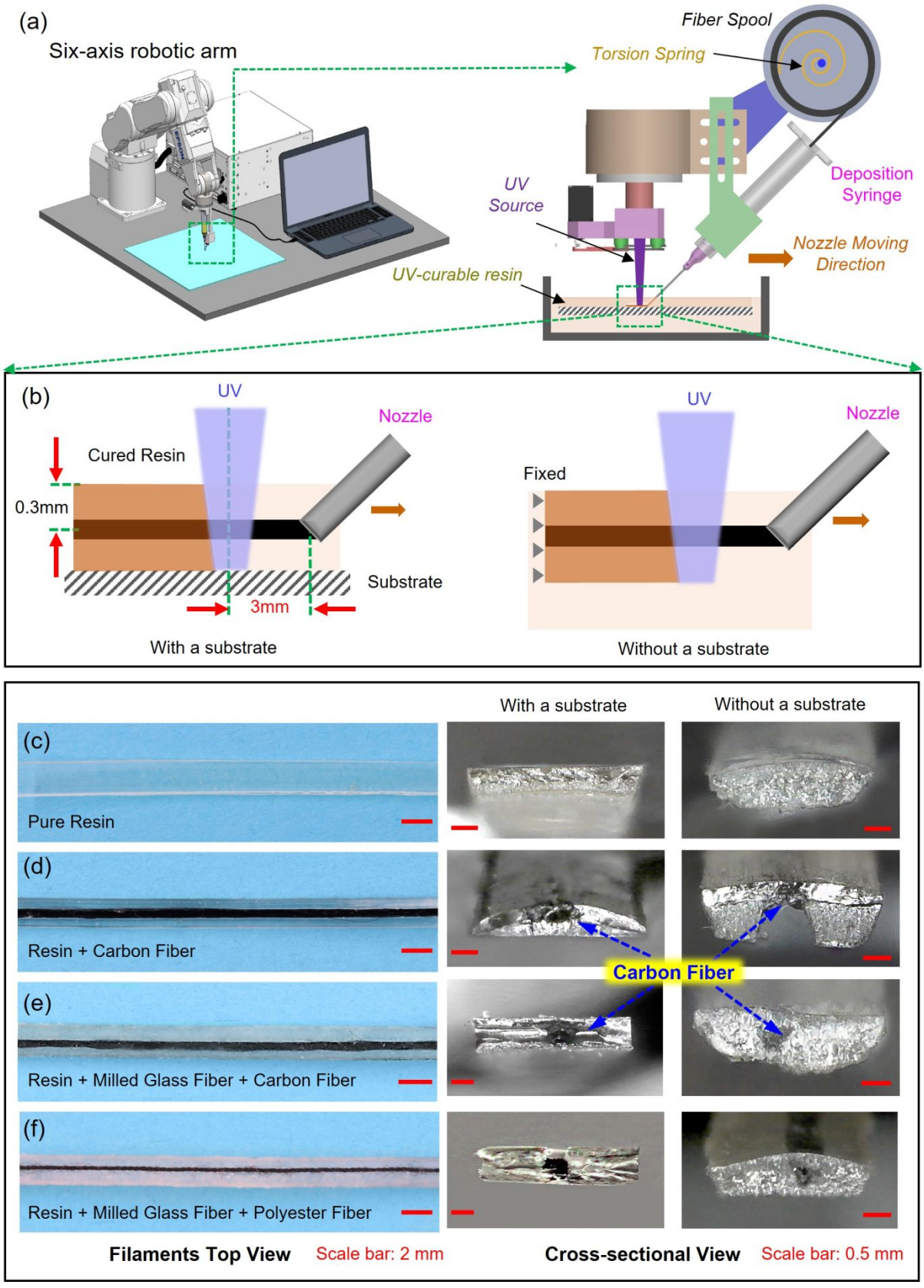

Figure 1. (a) A schematic view illustrating the experimental setup of embedded composite printing. (b)

Schematic view showing filament printing with and without a substrate. (c)-(f) Top view (left) and cross-sectional view (right) of printed filaments with different types of matrix resin and continuous fiber.

2.2 Embedded Printing of Composite Lamina and Laminate

Single-layer composite lamina samples are printed onto a glass substrate positioned 1 mm below the resin surface. In addition to adjusting the size of the applied laser beam, the filament spacing can be varied within a range from one to half of the beam width. This provides an effective parameter for controlling the fiber volume fraction (refer to **Figure 2a** for a schematic view and **Figure S2** for an experimental picture). A smaller filament spacing not only increases the fiber volume fraction but also enhances interfacial bonding between adjacent filaments. This is because the laser beam can cover previously deposited filaments, which further cures their matrix material and promotes filament interfacial polymerization.

Figure 2b shows a printed lamina sample with 2 mm filament spacing and a 3.6% fiber volume fraction. In the supplementary material, **Figure S3** displays lamina samples with 1.5 mm and 1 mm filament spacings, whose fiber volume fractions are 6.0% and 9.6%, respectively. It is observed that the carbon fibers in these samples are perfectly aligned without notable spreading issues. The embedded printing setup also allows for the fabrication of multilayer composite samples. A z-axis control mechanism is integrated to regulate the motion of the printing substrate within the resin tank. After printing one layer, the substrate is lowered by 1 mm and paused for 1 minute, allowing the resin to fully cover the surface before printing the next layer. **Figure 2c** shows a two-layer 0°/90° symmetric composite laminate with 1 mm filament spacing and a 9.6% carbon fiber volume fraction. In addition to carbon fibers, **Figure 2d** shows a printed single-layer lamina with 2.1% polyester fiber. The Supplementary Materials (**Figure S4**) include an image of a three-layer composite sample containing the same amount of polyester fiber.

The cross-sections of these printed composite samples were examined using an optical microscope and are presented in **Figure 2b** and **Figure 2d**. It is observed that the continuous fiber is precisely positioned along the sample's thickness direction, with no notable interfaces between adjacent filaments. The continuous fiber bundle is evenly spaced within the sample, and the lamina exhibits a remarkably flat surface. This is in great contrast to existing DIW printing methods, where printed samples often exhibit uneven, wavy surfaces due to the filament cylindrical shapes, even with careful control of resin viscosity and filament spacing. Maintaining a flat sample surface

is important to ensure the smooth printing process of CFRPs with a consistent gap between the needle tip and substrate layers. More importantly, it helps minimize void formation between adjacent printing layers within the printed composite structures, as demonstrated in the cross-sectional view of the multilayer composites in **Figure S4**. By measuring the composite densities, the multilayer composite samples in **Figure 2c** and **Figure S4** exhibit minimal void densities of 1.2% and 0.9%, respectively, which are significantly lower than the 14% void density reported in previous studies using conventional DIW printing methods [19].

Figure 2e shows the cross-sectional view of the printed composite laminas under a scanning electron microscope (SEM, Phenom Pharos G2 Desktop). When composites are printed with a 1k carbon fiber bundle and transparent resin, they exhibit an outstanding degree of fiber impregnation. This is primarily because the thin fiber bundle allows the low-viscosity resin to fully permeate the fibers before curing. However, when printing with a 6k fiber bundle, notable microscale voids are observed within the fiber bundle. This occurs because the thicker fiber bundle creates a greater obstacle, blocking UV transmission and hindering the curing of the matrix resin. SEM observations suggest that this issue can be resolved by using an opaque resin or by adding milled glass fiber to the resin to enhance light transmission through scattering. As a result, the printed samples exhibit minimal void formation and excellent fiber impregnation in their cross-sectional view.

It is noteworthy that when printing with resin containing milled glass fiber, the sample fracture surface exhibits distinct features. Specifically, the fracture morphology shows star-shaped patterns around individual fiber filaments. These features may be attributed to the unique fracture behaviors induced by the glass fiber additives, such as the yielding and notable plastic deformations of the matrix material. This observation warrants further investigation to fully understand the underlying mechanisms and their impact on the composite's properties.

The fiber volume fractions of printed laminas are characterized using different printing parameters. **Figure 2f** summarizes the fiber volume fractions as a function of filament spacing, with samples printed at a constant nozzle speed of 5 mm/s. It is observed that when printing with a 1k continuous fiber bundle, the fiber volume fraction increases linearly as the filament spacing (or the size of the laser beam) is reduced. The maximum volume fraction achieved is approximately 16.2%. By using a 6k fiber bundle with 0.6 mm filament spacing, the fiber volume fraction increases further to around 24%. It is important to note that when printing with thicker fiber bundles, the laser beam size must be at least larger than the width of the fiber bundle to ensure

complete coverage and wrapping by the matrix resin. The fiber volume fraction can be further increased by using a smaller deposition needle. Consequently, the size of the laser beam and the filament spacing can be reduced further while maintaining high-quality composite printing.

In **Figure 2g**, the fiber volume fractions are tested with different nozzle traveling speeds, ranging from 5 mm/s to 17 mm/s. Notably, the fiber content remains independent of the printing speed. This is because the amount of cured matrix around the fiber is predominantly determined by the size of the laser beam. However, it is crucial to ensure that the nozzle moving speed allows for sufficient resin curing. Excessively fast printing speeds result in insufficient UV irradiation and gel-like matrix material. In such cases, a subsequent post-curing process under UV light is necessary to fully polymerize the composite matrix.

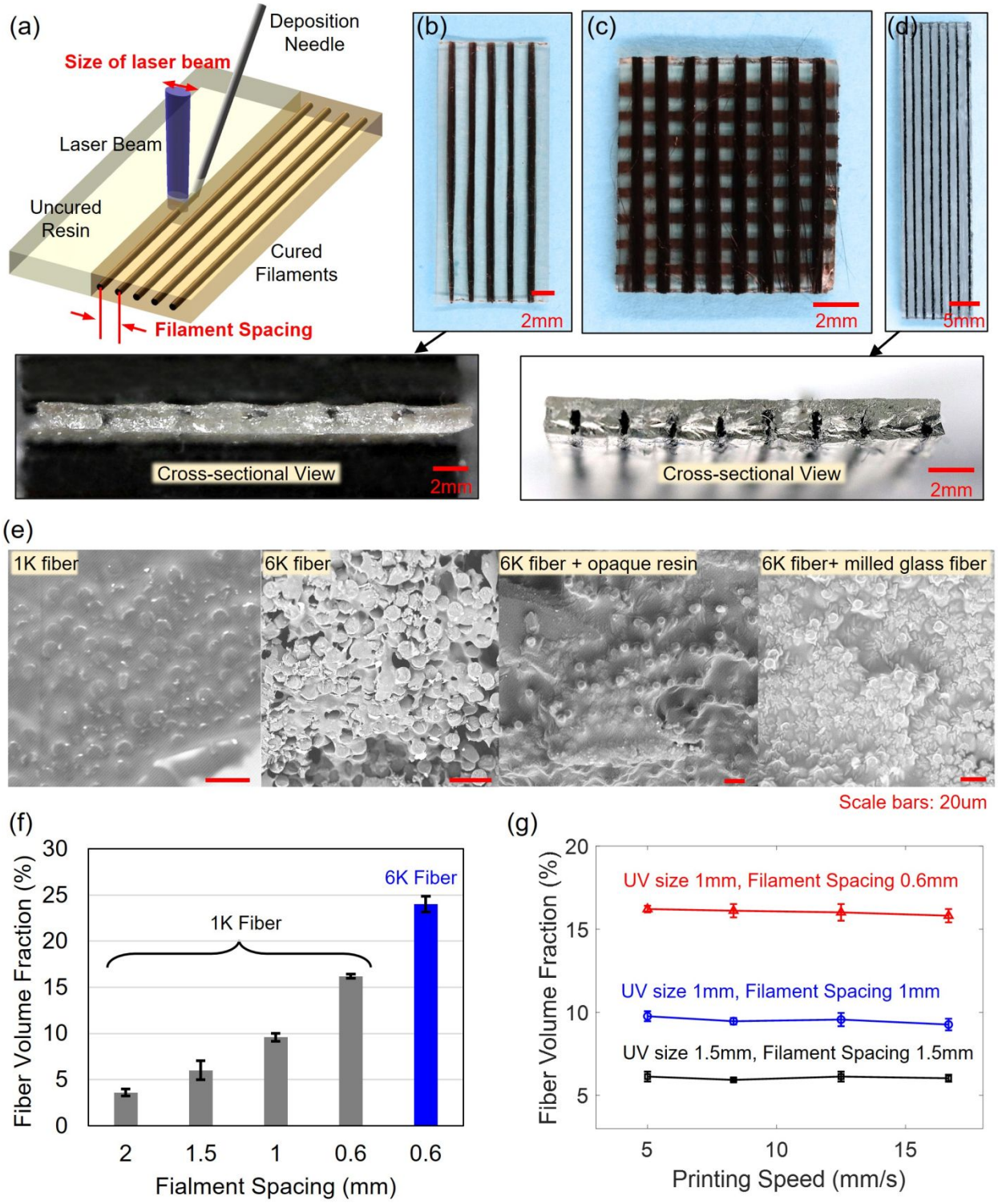

Figure 2. (a) A schematic view of the embedded composite printing highlighting the size of the applied laser beam and filament spacing. (b) A printed single-layer composite lamina with 3.6% carbon fiber and the sample cross-sectional view under microscope. (c) A two-layer 0°/90° symmetric composite laminate

with 9.0% continuous carbon fiber. (d) A printed single-layer composite lamina with 2.1% polyester fiber and the sample cross-sectional view under microscope. (e) SEM observations of composite laminas with different types of fiber bundle and matrix resins. (f) Summary of the fiber volume fraction of composite lamina with different printing speeds. (g) Summary of the fiber volume fraction of composite lamina with different printing speeds.

Uniaxial tension tests were conducted at room temperature to assess the mechanical properties of printed composite laminas with continuous carbon fibers. Rectangular samples were prepared according to the ASTM D3039 standard, which measure 10 mm in width and 80 mm in length. This was achieved by printing a large piece of lamina and then cutting it to the specified dimensions. To ensure excellent fiber impregnation in all samples, the opaque resin "Easy Grey" was used for embedded printing, which has identical thermomechanical properties as the transparent resin. The thickness of the printed single-layer lamina sample was approximately 1.3 mm. For each case, five identical samples were tested, and their average mechanical properties were reported.

The representative longitudinal and transverse stress-strain curves of laminas with different fiber volume fractions are presented in **Figure 3a** and **Figure 3b**, respectively. Specifically, the samples with 24% carbon fiber were printed using a 6k fiber bundle, while other samples were printed using a 1k bundle. When stretched in the longitudinal direction, the samples exhibited nearly constant stiffness until fracture. The fractures observed in all samples are attributed to the breakage of continuous carbon fiber, which indicates robust bonding between the fiber and polymer matrix. The incorporation of continuous carbon fiber dramatically enhances the mechanical properties. For example, according to the supplier, the matrix material without fiber reinforcement has an elastic modulus of 1.2 GPa and a fracture strength of 50 MPa. For the printed composites with a 24% fiber volume fraction, the longitudinal modulus is 37 GPa, and the fracture strength is 413 MPa, which represents 30-fold and 8.3-fold enhancements, respectively. Compared to the failure strain of 32% for the matrix resin, the failure strain of the printed lamina shows a notable decrease as the fiber content increases. On the other hand, the transverse tress-strain curves of printed laminas are shown to be nonlinear with a yielding point at around 2% strain. This is attributed to the plastic deformation of matrix materials when the laminas were stretched in the transverse direction. The transverse failure strains (up to 10%) are much higher than in the longitudinal direction.

The longitudinal and transverse modulus and ultimate strength of printed lamina samples are summarized in **Figure 3c** to **Figure 3f**. The lamina elastic moduli were calculated within the initial 0.5% engineering strain. To establish a comprehensive understanding of the material's mechanical characteristics, these two figures also include stiffness and strength of 3D printed laminas using other printing methods or matrix resins, including FDM printed thermoplastics composites [3, 28-31] and DIW printed thermosetting composites [15, 16, 19-22, 25, 32, 33], all containing continuous carbon fibers as reinforcements. The thermosetting composites include various matrix resins, such as thermally curable polyimine [15], one-stage [15, 16, 19-22] and two-stage [32, 33] UV-curable resins, and an aerospace-grade resin [25]. Specifically, the two-stage UV-curable resin can be rapidly cured upon UV irradiation during printing, followed by a thermal treatment step to enhance filament bonding through interfacial polymerization.

First, it is observed that in the longitudinal direction, both the lamina modulus and ultimate strength reported in this study are among the highest compared to other CFRPs at equivalent fiber volume fractions, especially those printed using thermoplastic matrix materials. This is primarily due to the highly straight and aligned continuous fibers with an outstanding degree of fiber impregnation in the printed composites. The figures show that their longitudinal moduli closely match predictions from the Rule of Mixtures (ROM).

The remarkable mechanical properties of embedded printed composites are evident in the transverse direction. As shown in **Figure 3e**, the transverse moduli of these laminas range from 1.20 GPa to 1.52 GPa, which is 8-10 times higher compared to DIW printed laminas using conventional UV-curable resins (0.15 GPa to 0.20 GPa) [19] and 2.3-4.8 times higher than those with a two-stage UV-curable resin (0.4 GPa to 0.66 GPa) [32]. The transverse moduli of embedded printed CFRPs are comparable to or even slightly higher than DIW printed laminas with a thermally curable polyimine matrix, and they also closely match ROM predictions.

Embedded printing also substantially enhances the transverse strength of laminas. As shown in **Figure 3f**, conventional DIW printed UV-curable composites exhibit transverse strengths around 1-1.2 MPa, while embedded printing dramatically enhances transverse strengths to 11-16 MPa, which represents over a tenfold increase. The projected strength could potentially match those of aerospace-grade UV-curable composites, as studied by Baur et al. [25]

The significantly enhanced transverse properties of printed lamina can be attributed to the minimal void formation and strong covalent bonding among composite filaments. During the

printing process, UV irradiation cures the current filaments and triggers interfacial polymerization among adjacent filaments. As a result, the filaments exhibit robust bonding, and the composites demonstrate high stiffness. Although the fibers used in this study are untreated on their surfaces, they still achieve strong bonding with the matrix materials due to excellent impregnation. Furthermore, because our printing speed is moderate, there is negligible friction around the needle tip, which prevents damage during the transportation of continuous fibers, as shown in **Figure 2.** These enhanced transverse properties of printed CFRPs represent a significant breakthrough in addressing a longstanding challenge in the field, as composites printed using extrusion-based methods typically exhibit weak bonding strength among filaments and layers.

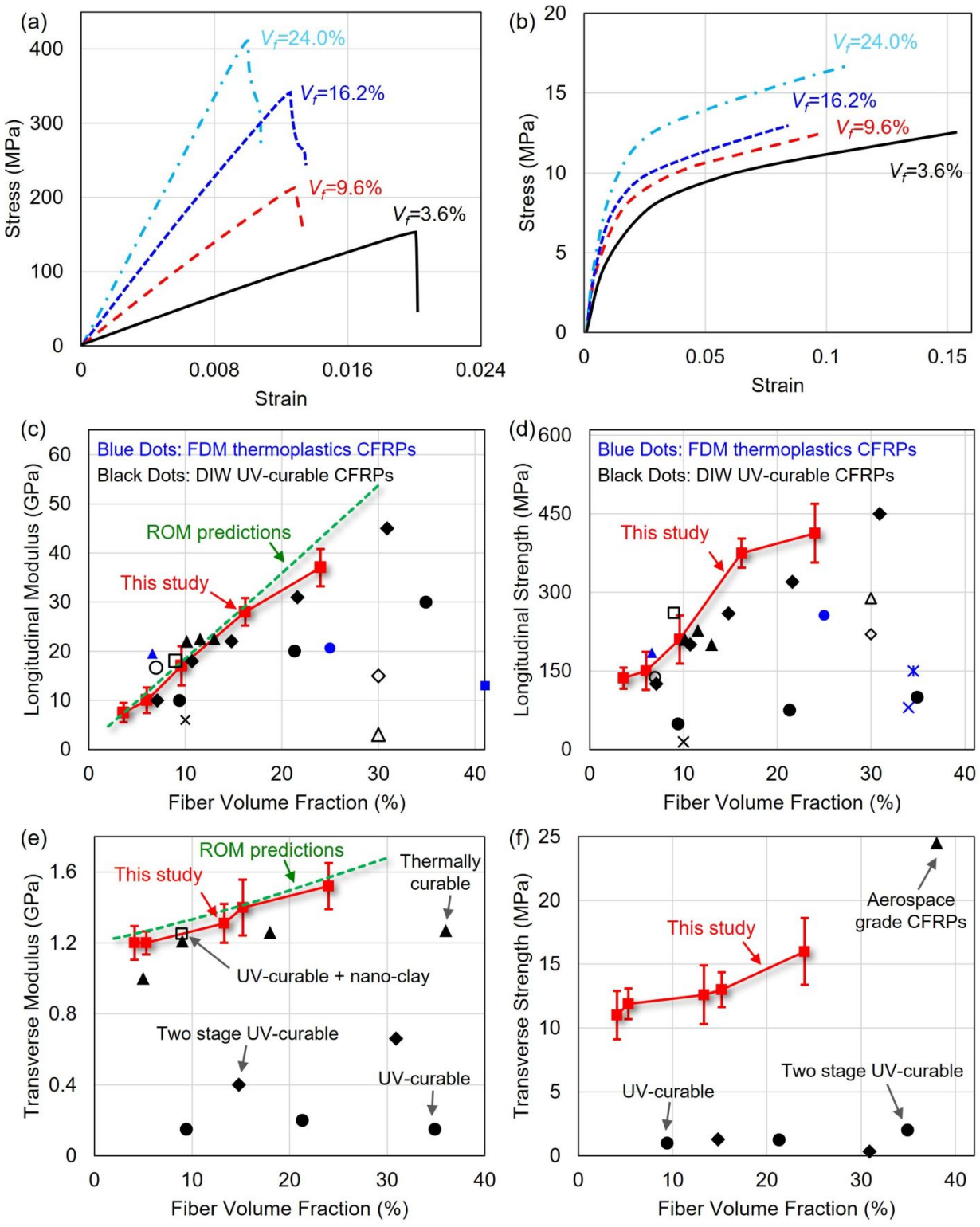

Figure 3. Mechanical properties of composite lamina fabricated using the embedded printing method. (a) (a) Representative longitudinal and (b) transverse stress-strain curves of laminas with different fiber volume fractions. Summary of (c) longitudinal moduli, (d) longitudinal strength, (e) transverse moduli, and (f)

transverse strength of printed laminas. In these figures, the data of FDM printed thermoplastic composites is sourced from Ref. [3, 28-31]. The data of DIW printed UV curable composites, thermally curable composites, and aerospace grade composites are respectively sourced from Ref. [15, 16, 19-22, 32, 33], Ref. [15], and Ref. [25].

2.3 Unique Capability I: Dynamically Control Fiber Volume Fraction during Printing

The developed embedded printing method offers several unique capabilities that can greatly benefit composite manufacturing, which are not achievable with existing extrusion-based methods. The first capability is the flexibility to dynamically control the fiber volume fraction during printing. This is achieved by adjusting the size of the laser beam, which controls the amount of resin cured around the fiber bundle.

As illustrated in **Figure 4a**, a mechanism has been designed to regulate the spot size of the laser beam. This is accomplished through a programmable Arduino that controls the rotation of the gear, thereby adjusting the aperture's opening size. The intensity of the applied UV light remains fixed throughout the printing process. **Supplementary Video 3** shows the printing process of a composite filament with a gradually decreasing size of the laser beam. **Figure 4b - Figure 4d** show several printed composite filaments with varying fiber volume fractions along the axial direction. These filaments were printed at a speed of 5 mm/s, and the boundary of their matrix materials precisely matches the size profile of the applied laser beam. **Figure 4e** shows two cross-intersecting composite filaments with varying fiber volume fractions to form a windmill configuration.

The demonstrated capability of dynamically controlling the fiber volume fraction has great potential for fabricating advanced composites and structures with highly optimized topology and fiber distributions. For example, there is increasing interest in using topology optimization techniques to design composites with tailored mechanical properties [34-38]. In these studies, both composite topology and fiber volume fractions are treated as design variables [35, 39-42]. The resulting designs require laying composite filaments with varying fiber volume fractions in space, which is unlikely to be achieved using conventional DIW printing methods with a fixed nozzle diameter. The embedded printing method developed in this study significantly reduces manufacturing constraints and allows for the efficient fabrication of such optimized composite structures. Furthermore, the high printing quality is expected to yield mechanical properties close to the target performances predicted under “defect-free” assumptions.

In addition to controlling in-plane stiffness, the developed printing method enables the fabrication of composite components with tailored out-plane stiffness. As a demonstration, **Figure 4f** illustrates the stable configurations of a 3D printed bistable compliant structure, where the strip members on both sides are the printed composite filaments with controlled volume fractions of carbon fiber. Upon compressive loading, the compliant structure rapidly transitions from one stable position to the next when the strip members are bent [43-46], with their bending stiffness determining the overall structural responses. The corresponding force-displacement relationships are presented in **Figure 4g**. When the composite filament in **Figure 4c** is employed, the structure exhibits a critical buckling load of 1.95 N, a snap-through point at 8.4 mm, and a second stable configuration at 13.9 mm. However, when merging the two thin sections of the filament into one middle section while maintaining the same macroscopic length, the structure displays steady nonlinear deflections without bistable configurations. This simple demonstration highlights the potential of the developed 3D printing method to fabricate structures (or functional components) with highly tunable bending stiffness, which hold promise for diverse applications, including microelectromechanical systems, aerospace components, robotics, medical devices, etc.

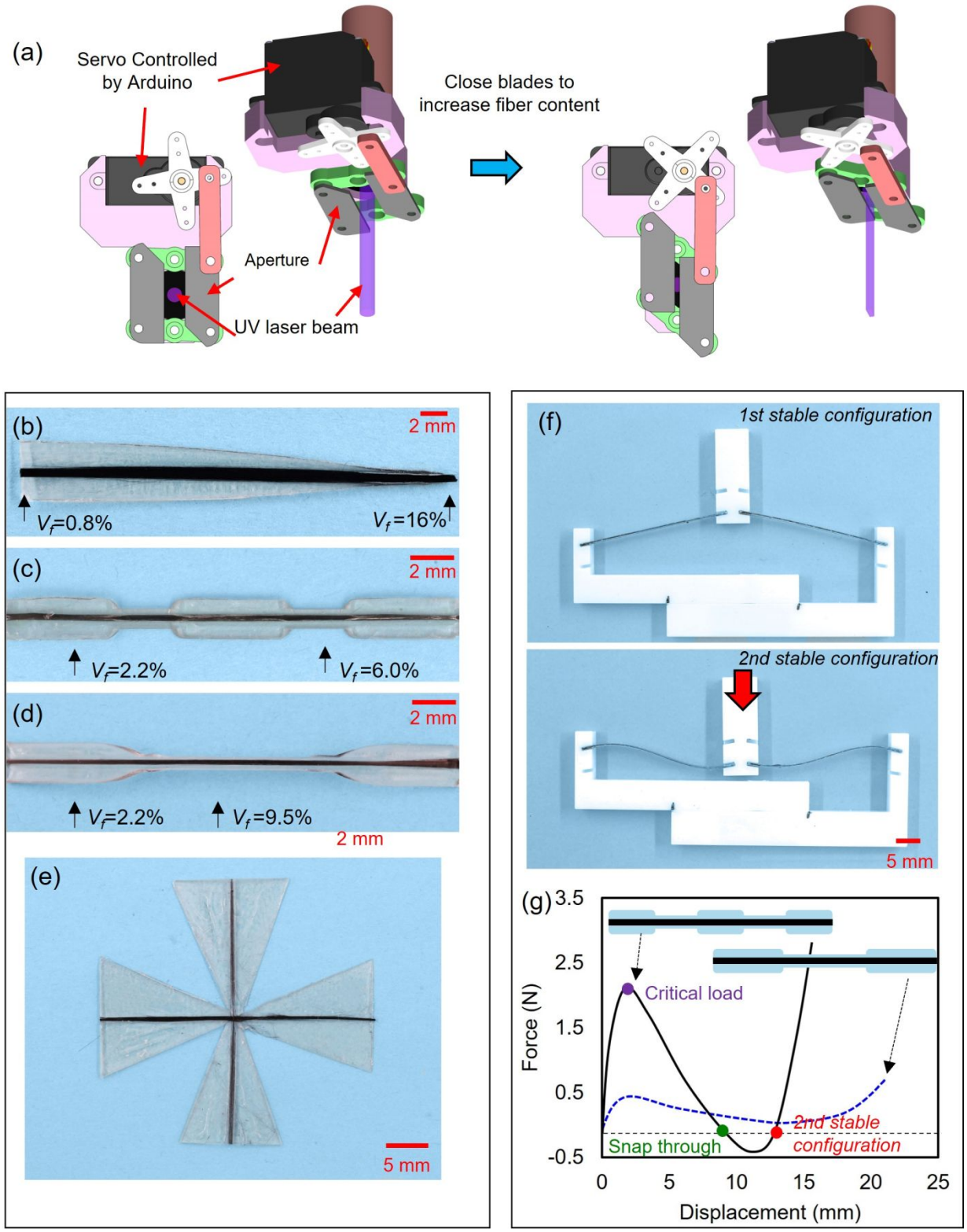

Figure 4. (a) A schematic view illustrating the mechanism for dynamically controlling the size of the laser beam and, consequently, the fiber volume fraction during printing. (b)-(d) Printed composite filaments

showcasing varying fiber volume fractions along the axial direction. (e) Cross-intersecting composite filaments with varying fiber volume fractions. (f)-(g) A 3D printed bistable compliant structure and the corresponding force-displacement relationships.

2.4 Unique Capability II: Switch Matrix Materials during Printing

The second unique capability of the embedded printing method is its ability to switch matrix materials without cutting the continuous fibers during the composite printing process. This is a highly desirable feature for 3D printing multi-material and multifunctional composites, but it is unattainable with existing extrusion-based methods. The schematic views in **Figure 5a** illustrate the working mechanism. After printing with the first resin, the printing process is temporarily paused, and the external laser beam is turned off. The initial resin is removed from the tank through negative pressure. Any residual resin on the sample surface is then carefully cleaned using tissue paper. Subsequently, the tank is refilled with a second resin up to the same height to resume the printing.

Figure 5b shows several printed filaments embedded with continuous carbon fiber, where the spot size of the laser beam is set to be 2 mm during printing. These filaments are printed using two different resins with different colors and stiffness along the axial direction. Specifically, the fully cured black matrix is a soft material with a room-temperature modulus of approximately 800 MPa. To demonstrate the capabilities, the length of the different material sections gradually decreases. It is observed that even with the smallest length of 3mm, the boundaries of the different sections remain clearly visible, and there are no notable contaminations of the matrix materials. The multimaterial distribution results in the printed filaments exhibiting non-uniform bending curvatures.

In **Figure 5c**, composite samples are printed through dynamically controlling both fiber volume fraction and matrix materials. Each sample comprises four cross-intersecting composite filaments with continuous carbon fiber. In addition to the use of different matrix materials, the filament width is regulated to increase linearly along the radial direction. In the right sample, the evolution of the filament width is designed and precisely controlled, resulting in the formation of printed composites that take the shape of a closed circular disc. Both printed samples demonstrate a high printing resolution with perfectly aligned fibers and well-defined material boundaries.

To evaluate the interfacial bonding strength between the different matrix materials, a lamina sample is printed using two distinct matrix materials (the soft "*Clear 65D"* and the stiff "*Easy Grey*"), as demonstrated in **Figure 5d**. The cross-sectional view indicates no notable void formations or microscale defects around the material interfaces. The printed sample is trimmed and subjected to room-temperature uniaxial tension tests in the transverse direction. Notably, the appearance of the sample after fracture suggests (**Figure 5e**) that the failure occurred on the side with the soft matrix material, rather than at the material interfaces. The corresponding stress-strain curve is presented in **Figure 5f**, which is also compared to the stress responses of a lamina sample printed with the soft matrix material. It is observed that the ultimate strength and failure strain of the composite sample are close to those of the single-material lamina. These characterizations suggest a robust bonding strength between different matrix materials during the embedded composite printing.

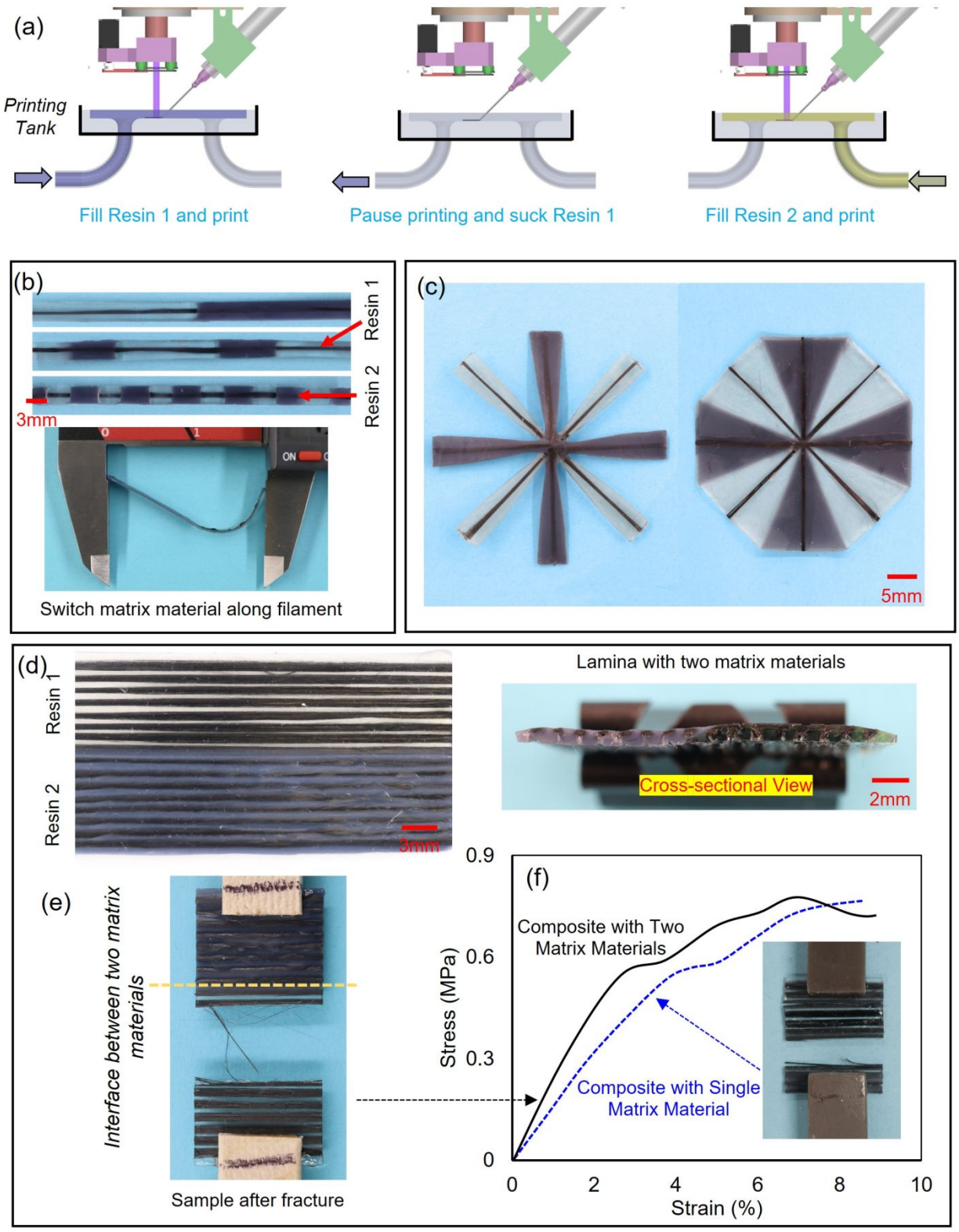

Figure 5. (a) A schematic view showing the mechanism to dynamically change the matrix materials during the printing. (b) Several printed composite filaments with different matrix materials along the axial direction.

(c) Composite samples printed by dynamically controlling both fiber volume fraction and matrix materials. (d) A lamina sample printed with two different materials. (e) The appearance of the sample after fracture. (f) Corresponding stress-strain curves in the transverse direction.

2.5 Unique Capability III: Printing of Composite Structures with Overhanging Filaments

The third unique capability of the embedded printing method is its ability to effectively print overhanging filaments without support materials, which is essential for creating advanced composite structures, such as hollow designs. Before exploring this capability, we first examine the method's ability to print filaments along curved pathways, which is another crucial requirement for 3D printing composite structures.

The sixth joint of the adopted robotic arm enables the continuous rotation of the printhead and allows for the printing of composite filaments along intricate paths. **Figure 6a - Figure 6c** show composite filaments printed along trigonometric sine, cosine, and tangent curves. The analytical printing pathway from the CAD model is also marked in the figures for comparison. The small deviation observed suggests a high capability for printing composite structures with well-defined fiber positioning and filament boundaries. These filaments were printed using a 1k fiber bundle with a fiber volume fraction of around 3.6%. However, when printing with a higher fiber volume fraction or around sharp corners, the embedded fibers tend to deviate from the intended path due to their intrinsic stiffness, and significant residual stress may develop after curing. For example, **Figure S5** shows printed composites with straight segments and sharp turns, such as a five-pointed star, a squared spiral, and a zigzag pattern. While the printed composites exhibit outstanding overall quality, slight deviations are observed in the continuous fiber layout at the sharp corners. The maximum printable curvature of composite filaments depends on various material and printing parameters, such as fiber stiffness, fiber content, and UV intensity, which warrants a future rigorous study.

When printing overhanging composite filaments without a substrate, the buoyancy of the filaments within the resin effectively counterbalances gravitational forces. This feature enables the creation of composite structures with hollow designs without the need for support materials, which simplifies the manufacturing process and reduces material waste. **Figure 6d** and **Figure 6e** illustrate composite filaments printed between two substrates with an increasing span distance from 1cm to 15cm. These structures are respectively produced using the conventional in-nozzle

impregnation DIW printing method [19] and the embedded printing method developed in this study. In the embedded printing approach, the entire substrate structure is immersed in the resin tank. It is observed that with the increasing span distance, the DIW-printed filaments exhibit noticeable deflection. The maximum deflection at the middle points reaches up to 8mm, which is comparable to the length of the filaments. In contrast, overhanging filaments created with the embedded printing method exhibit negligible deflection. This comparison highlights the advantage of the developed printing technology in producing stable and precise overhangs without the need for additional support.

In **Figure 6f**, we extend this concept by printing a layer of composite lamina with continuous polyester fiber to cover the top of an open box, which mimics the actual processes involved in printing composite structures with hollow features. The newly added composite layer maintains great stiffness and interfacial bonding with the substrate materials. It exhibits negligible deflection even when subjected to an external weight of 250 grams. In **Figure 6g**, a 3D lattice structure is demonstrated. The structure comprises perpendicular frame members laying over each other. Each member consists of two layers of composite filament printed in the height direction. The zoomed-in view of the figure highlights the details of the intersection points. The filaments are precisely printed between the standing points without collapsing or exhibiting notable deflections.

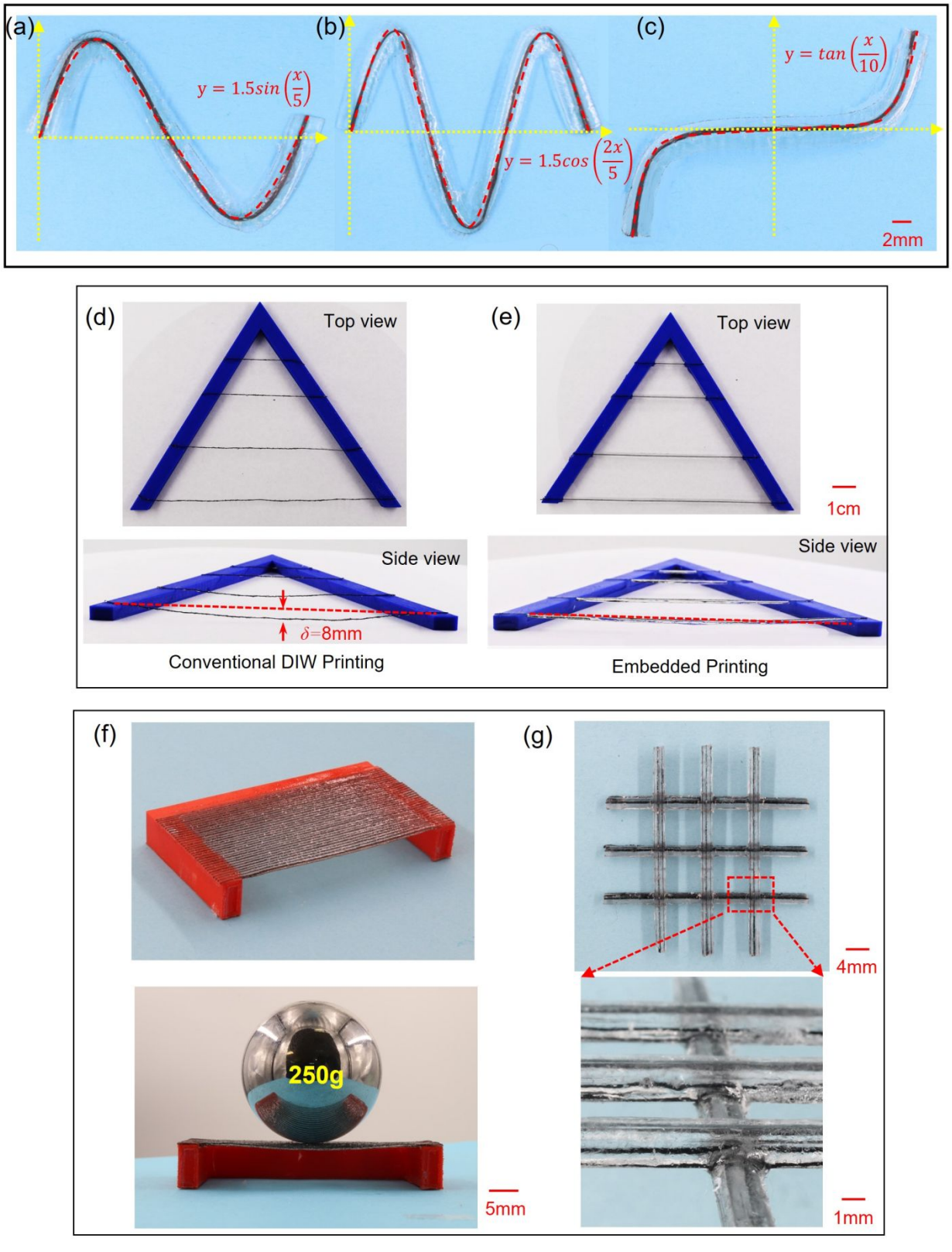

Figure 6. (a)-(c) Composite filaments printed along trigonometric sine, cosine, and tangent curves. The red dashed curves are the analytical printing pathways from the CAD model (d)-(e) Composite filaments

printed between two substrates using conventional in-nozzle impregnation DIW printing method and the embedded printing method. (f) A layer of composite lamina printed with continuous polyester fiber to cover the top of an open box. (g) A 3D lattice structure with continuous polyester fiber.

3. Conclusion

In summary, this study introduces an innovative embedded 3D printing technique for UV-curable composites with continuous fiber, which eliminates the significant manufacturing constraints of conventional extrusion-based printing methods, allowing the unique design and manufacturing capabilities of 3D printing to be fully utilized for fabricating contemporary composites with highly optimized topology and distributions of fibers and matrix materials. It effectively resolves issues such as resin spreading or fiber loosening in conventional DIW methods and demonstrates the capability to create high-quality samples with perfectly aligned continuous fibers and minimal void density. The printed lamina samples exhibit outstanding mechanical properties in both longitudinal and transverse directions that are close to theoretical predictions and outperform those printed using conventional extrusion-based methods. The developed printing method enables the dynamic control of fiber volume fractions and changes of matrix resin during the printing, which releases notable manufacturing constrains for the design of highly optimized or multifunctional composites. Moreover, the printing process balances gravitational forces with the buoyancy of composite filaments in the resin, allowing for the fabrication of hollow structures without the need for support materials. Since the printing process does not require any chemical modifications of resins and reinforcement fibers, it is compatible with a wide range of feedstock materials and is anticipated to be an influential approach for future development of composites with diverse applications across various fields.

4. Experimental Section

Feedstock Materials and Embedded Composite Printing: A range of commercially available UV-curable resins were purchased from Siraya Tech Inc. (San Gabriel, CA) for the composite printing process. Specifically, the stiff resin used for printing composite filaments, lamina, and structures is either a transparent "*Clear V2*" or a non-transparent "*Easy Grey*" Blu-Tough resin. These resins exhibit identical mechanical properties: a 1.2 GPa Young's Modulus and a 32% failure strain. In Section 2.4, when demonstrating composite printing with different matrix materials, an additional

soft resin, "*Clear 65D*" Tenacious - Flexible resin, is used, which has a Young's Modulus of 800 MPa and a failure strain of 70%.

For the continuous fiber, the 1k carbon fiber bundle was purchased from CST - The Composites Store, Inc. (Tehachapi, CA), and the polyester fiber was purchased from Coats & Clark Inc. (London, UK). According to the suppliers, the Young's modulus for these fibers is 174 GPa and 3.5 GPa, respectively. The milled fiberglass with a 1/32-inch average length was purchased from FibreGlast Inc. (Brookville, OH). During the embedded composite printing process, the 405 nm UV light was provided by a 5mw laser dot (Qiaoba Inc., China). The motion of the printer head was controlled by an Epson C8 6-Axis Robots system (Los Alamitos, CA, USA).

Fiber Volume Fraction Measurement: The fiber volume fraction of printed composites was determined by measuring the weights of both the matrix materials and the embedded fiber. Specifically, the weight of the matrix materials is obtained by subtracting the composite weight from the weight of continuous fiber with the same length. Their volume ratio was then determined considering the material densities. According to the information provided by the suppliers, the densities of fully cured matrix resin, carbon fiber, and polyester fiber are 1.15 g/cm^3, 1.75 g/cm^3, and 1.38 g/cm^3, respectively.

Void Density Measurements: The porosities of the printed composite samples were determined by evaluating their density. Initially, the sample weight was measured both in the air and underwater. Subsequently, the sample volume and density were determined using Archimedes' principle. The sample porosities were then calculated based on the densities of the base polymer and fiber bundle.

Mechanical Characterizations: The mechanical properties of the printed composite lamina, including stress-strain relationships and elastic modulus, were assessed through uniaxial tensile tests at room temperature. The tests were performed using the MTS Insight® Electromechanical Testing Systems (MTS Systems Corporation, Eden Prairie, MN, USA). All tension tests were conducted at a strain loading rate of 2%/min. Following the tests, we calculated the initial elastic modulus within a 0.5% engineering strain range.

The glass transition temperature and storage modulus of the UV cured resin were characterized using a dynamic mechanical analysis (DMA) tester (Model Q800, TA Instruments, New Castle,

DE, USA). The characterization was performed at a frequency of 1 Hz and a strain level of 0.1%. Initially, the temperature was equilibrated at -10˚C for 5 min and then ramped up at a heating rate of 2˚C/min. The glass transition temperature (T_g) was determined as the temperature corresponding to the peak of the tan δ curve.

Conflicts of Interest

The authors have no conflicts of interest to disclose.

Data Availability

Data for this article is available upon request to the corresponding authors.

Acknowledgements

K.Y. and M.D. acknowledge the support of AFOSR grant (FA-20-1-0306; Dr. B.-L. "Les" Lee, Program Manager).

References

1. Cheng, P., et al., *3D printed continuous fiber reinforced composite lightweight structures: A review and outlook.* Composites Part B: Engineering, 2023. **250**: p. 110450.
2. Kabir, S.M.F., K. Mathur, and A.-F.M. Seyam, *A critical review on 3D printed continuous fiber-reinforced composites: History, mechanism, materials and properties.* Composite Structures, 2020. **232**: p. 111476.
3. Matsuzaki, R., et al., *Three-dimensional printing of continuous-fiber composites by in-nozzle impregnation.* Scientific Reports, 2016. **6**: p. 23058.
4. Sugiyama, K., et al., *3D printing of composite sandwich structures using continuous carbon fiber and fiber tension.* Composites Part A: Applied Science and Manufacturing, 2018. **113**: p. 114-121.
5. Chen, Y. and L. Ye, *Topological design for 3D-printing of carbon fibre reinforced composite structural parts.* Composites Science and Technology, 2021. **204**: p. 108644.
6. Fernandes, R.R., et al., *Experimental investigation of additively manufactured continuous fiber reinforced composite parts with optimized topology and fiber paths.* Additive Manufacturing, 2021. **44**: p. 102056.
7. Li, N., G. Link, and J. Jelonnek, *Rapid 3D microwave printing of continuous carbon fiber reinforced plastics.* CIRP Annals, 2020. **69**(1): p. 221-224.

8. Li, N., G. Link, and J. Jelonnek, *3D microwave printing temperature control of continuous carbon fiber reinforced composites.* Composites Science and Technology, 2020. **187**: p. 107939.
9. Luo, M., et al., *Impregnation and interlayer bonding behaviours of 3D-printed continuous carbon-fiber-reinforced poly-ether-ether-ketone composites.* Composites Part A: Applied Science and Manufacturing, 2019. **121**: p. 130-138.
10. Luo, M., et al., *Controllable interlayer shear strength and crystallinity of PEEK components by laser-assisted material extrusion.* Journal of Materials Research, 2018. **33**(11): p. 1632-1641.
11. Hao, W.F., et al., *Preparation and characterization of 3D printed continuous carbon fiber reinforced thermosetting composites.* Polymer Testing, 2018. **65**: p. 29-34.
12. Ming, Y.K., et al., *Investigation on process parameters of 3D printed continuous carbon fiber-reinforced thermosetting epoxy composites.* Additive Manufacturing, 2020. **33**.
13. Ming, Y., et al., *Self-heating 3D printed continuous carbon fiber/epoxy mesh and its application in wind turbine deicing.* Polymer Testing, 2020. **82**: p. 106309.
14. Wang, B., et al., *Fabrication of triangular corrugated structure using 3D printed continuous carbon fiber-reinforced thermosetting epoxy composites.* Polymer Testing, 2022. **106**: p. 107469.
15. He, X., et al., *3D printing of continuous fiber-reinforced thermoset composites.* Additive Manufacturing, 2021. **40**: p. 101921.
16. Rahman, M.A., et al., *3D printing of continuous carbon fiber reinforced thermoset composites using UV curable resin.* Polymer Composites, 2021. **42**(11): p. 5859-5868.
17. Ming, Y., et al., *Fabrication of continuous glass fiber-reinforced dual-cure epoxy composites via UV-assisted fused deposition modeling.* Composites Communications, 2020. **21**: p. 100401.
18. Kunze, E., et al., *Experimental studies for the additive manufacturing of continuous fiber reinforced composites using UV-curing thermosets.* 2021.
19. Abdullah, A.M., et al., *Direct-write 3D printing of UV-curable composites with continuous carbon fiber.* Journal of Composite Materials, 2023. **57**(4): p. 851-863.
20. Thakur, A. and X. Dong, *Printing with 3D continuous carbon fiber multifunctional composites via UV-assisted coextrusion deposition.* Manufacturing letters, 2020. **24**: p. 1-5.
21. Pappas, J.M., A.R. Thakur, and X. Dong, *Effects of cathode doping on 3D printed continuous carbon fiber structural battery composites by UV-assisted coextrusion deposition.* Journal of Composite Materials, 2021. **55**(26): p. 3893-3908.
22. Liu, W., et al., *Additive manufacturing of silicone composite structures with continuous carbon fiber reinforcement.* Polymer Engineering & Science, 2023. **63**(6): p. 1716-1724.
23. Tyler, K., *Method and apparatus for continuous composite three-dimensional printing*. 2012: USA.

24. Jiang, H., et al., *3D Printing of continuous fiber composites using two-stage UV curable resin.* Materials Horizons, 2023.
25. Baur, J.W., et al., *Mechanical properties of additively printed, UV cured, continuous fiber unidirectional composites for multifunctional applications.* Journal of Composite Materials, 2023. **57**(4): p. 865-882.
26. İpekçi, A. and B. Ekici, *Experimental and statistical analysis of robotic 3D printing process parameters for continuous fiber reinforced composites.* Journal of Composite Materials, 2021. **55**(19): p. 2645-2655.
27. Lu, Y., et al., *Continuous fibre reinforced Vat photopolymerisation (CONFIB-VAT).* Additive Manufacturing, 2022. **60**: p. 103233.
28. Goh, G.D., et al., *Characterization of mechanical properties and fracture mode of additively manufactured carbon fiber and glass fiber reinforced thermoplastics.* Materials & Design, 2018. **137**: p. 79-89.
29. Tian, X., et al., *Recycling and remanufacturing of 3D printed continuous carbon fiber reinforced PLA composites.* Journal of cleaner production, 2017. **142**: p. 1609-1618.
30. Van Der Klift, F., et al., *3D printing of continuous carbon fibre reinforced thermo-plastic (CFRTP) tensile test specimens.* Open Journal of Composite Materials, 2015. **6**(1): p. 18-27.
31. Li, N., Y. Li, and S. Liu, *Rapid prototyping of continuous carbon fiber reinforced polylactic acid composites by 3D printing.* Journal of Materials Processing Technology, 2016. **238**: p. 218-225.
32. Jiang, H., et al., *3D Printing of Continuous Fiber Composites Using Two-stage UV Curable Resin.* Materials Horizons, 2023.
33. Rahman, M.A., et al., *A mechanical performance study of dual cured thermoset resin systems 3D-printed with continuous carbon fiber reinforcement.* Polymers, 2023. **15**(6): p. 1384.
34. Boddeti, N., et al., *Simultaneous Digital Design and Additive Manufacture of Structures and Materials.* Scientific Reports, 2018. **8**.
35. Boddeti, N., et al., *Optimal design and manufacture of variable stiffness laminated continuous fiber reinforced composites.* Scientific Reports, 2020. **10**(1): p. 16507.
36. Li, N., et al., *Path-designed 3D printing for topological optimized continuous carbon fibre reinforced composite structures.* Composites Part B: Engineering, 2020. **182**: p. 107612.
37. Xia, L. and P. Breitkopf, *Concurrent topology optimization design of material and structure within FE2 nonlinear multiscale analysis framework.* Computer Methods in Applied Mechanics and Engineering, 2014. **278**: p. 524-542.

38. Sivapuram, R., P.D. Dunning, and H.A. Kim, *Simultaneous material and structural optimization by multiscale topology optimization.* Structural and Multidisciplinary Optimization, 2016. **54**(5): p. 1267-1281.
39. Zhang, F., et al., *Topology Design of 3D Printing Continuous Fiber-Reinforced Structure Considering Strength and Non-Equidistant Fiber.* Advanced Engineering Materials, 2024. **26**(1): p. 2301340.
40. Fernandez, F., et al., *Optimal design of fiber reinforced composite structures and their direct ink write fabrication.* Computer Methods in Applied Mechanics and Engineering, 2019. **353**: p. 277-307.
41. Zhang, X., et al., *A nodal-based optimization method for the design of continuous fiber-reinforced structures.* Composite Structures, 2023. **323**: p. 117455.
42. Sugiyama, K., et al., *3D printing of optimized composites with variable fiber volume fraction and stiffness using continuous fiber.* Composites Science and Technology, 2020. **186**: p. 107905.
43. Zirbel, S.A., et al., *Bistable mechanisms for space applications.* PloS one, 2016. **11**(12): p. e0168218.
44. Homer, E.R., et al., *New methods for developing and manufacturing compliant mechanisms utilizing bulk metallic glass.* Advanced Engineering Materials, 2014. **16**(7): p. 850-856.
45. Jagtap, S., B. Deshmukh, and S. Pardeshi. *Applications of compliant mechanism in today's world–A review*. in *Journal of physics: conference series*. 2021. IOP Publishing.
46. Liu, T. and G. Hao, *Design of deployable structures by using bistable compliant mechanisms.* Micromachines, 2022. **13**(5): p. 651.

Data Availability

Data for this article is available upon request to the corresponding authors.